

Underwater Wet Welding for HSLA Steels: Chemical Composition, Defects, Microstructures, and Mechanical Properties

Wen-Bin Gao¹ · Dong-Po Wang¹ · Fang-Jie Cheng¹ · Cai-Yan Deng¹ · Wei Xu²

Received: 20 March 2015 / Revised: 23 June 2015 / Published online: 25 July 2015
© The Chinese Society for Metals and Springer-Verlag Berlin Heidelberg 2015

Abstract The effect of water depth on underwater wet welds was investigated by underwater wet shielded metal-arc welding technique. The microstructures, chemical composition, welding defects, and mechanical properties were studied. The contents of alloying elements decrease, while the oxygen content increases with water depth. Within 55 m depth, the carbon monoxide reaction is controlling the oxygen content which will further control the contents of alloying elements. The columnar microstructures in weld metal obtained at shallow water consist of grain boundary ferrite, side-plate ferrite, and acicular ferrite, while those at depth greater than 11 m exhibit more proeutectoid ferrite due to the loss of alloying elements. Mechanical properties are a strong function of depth owing to the increase in oxidation of alloying elements and porosity. Welds obtained within 11 m show preferable strength, ductility, and toughness. The mechanical properties significantly drop from 11 to 25 m because of the increased porosity and oxidation of alloying elements.

KEY WORDS: Underwater wet welding; Electrode; High-strength steel; Microstructures; Mechanical properties

1 Introduction

The increasing global energy demand continues to push oil companies into deeper and deeper waters in search of economically recoverable reserves of oil and gas [1–3]. However, for the marine structures, the effects of the elements and applied loads potentially result in unsafe conditions. In general, it is often too expensive or even impossible to move the damaged structures to the land. Therefore, underwater welding of high-strength low-alloy

(HSLA) steels is a promising technique in the in situ repairs of maritime structures [4, 5].

Due to the versatility and the low cost compared with other underwater welding techniques, underwater wet welding (UWW) has been widely used for many years in the repair of offshore platforms, especially for the depth <60 m [6]. Many papers have been reported on this technique. Ezequiel et al. [7] investigated the influence of porosity variation on the properties of multipass V-groove weld obtained by a gravity feeding system at 50 and 100 m depths. They found that porosity reduced along the weld length in multipass wet welds and it was a factor responsible for the mechanical properties' variation. Perez et al. [8] reported that nickel addition to rutile-grade electrodes of approximately 2% (wt.) improves the toughness of underwater wet welds to 60 J at 0 °C. Zhang et al. [9] investigated the effect of the real-time induction heating process on the underwater FCAW wet joint. The process reduced the cooling rate of the joint and improved the arc stability, the mechanical properties, and the susceptibility to cold cracking.

Available online at <http://link.springer.com/journal/40195>

✉ Fang-Jie Cheng
chfj@tju.edu.cn

¹ Tianjin Key Laboratory of Advanced Joining Technology, School of Materials Science and Engineering, Tianjin University, Tianjin 300072, China

² Offshore Oil Engineering Co., Ltd, Tianjin 300072, China

The most widely applied standard in evaluating the underwater welds is AWS D3.6 M: 2010 [10]. Three weld classes (A, B, and O), which encompass the range of quality and properties currently produced by application of the various methods, are specified in the standard. Class A welds are intended to be suitable for applications and design stresses comparable to their conventional surface welding counterparts. Class B welds are intended for less critical applications where lower ductility, moderate porosity, and other limited discontinuities can be tolerated.

DH36 steel is widely applied in the construction of ship and offshore platforms, and oil or natural gas pipelines usually utilize X65 steel for its high strength and good corrosion resistance. In the present work, these two HSLA steels are selected as base metals. The macro- and microstructures of the welds are investigated. According to the class B weld standard, the mechanical properties of joints welded within 55 m water depth are studied. The purpose of this paper is to provide the direction and guidance for marine structure maintenance using underwater wet shielded metal-arc welding technique in different water depths.

2 Experimental

2.1 Materials and Equipment

The materials investigated in the present study are DH36 and X65 steel plates both with 12.7 mm thickness, and the carbon equivalents are 0.373 and 0.313, respectively, according to IIW. The nominal chemical composition and mechanical properties are listed in Tables 1 and 2, respectively. The microstructures of both DH36 and X65 consist of polygonal ferrite and pearlite, and the grain size of X65 is much smaller. The filled material used here is a commercial E7014 rutile underwater electrode with a diameter of 3.2 mm. The covering is mainly composed of iron powder and titania, and the waterproofing is wax. The content of diffusible hydrogen (welded at 0.5 m) is 46.72 mL/100 g tested by a gas chromatography analyzer. The mechanical properties are also listed in Table 2.

The weld joint was composed with two DH36 or X65 steel sheets (280 mm × 150 mm × 12.7 mm) and one

Table 2 Mechanical properties

Material	Yield strength (MPa)	Tensile strength (MPa)	Elongation rate (%)
UW-CS-1*	476	523	8.0
DH36	380	520	30
X65	510	580	44

Results were obtained from an all-weld-metal tension specimen welded at 2 m by diver welder

* shows that the yield/ultimate strength and elongation rate is obtained by an all-weldmetal tension specimen welded at 2 m water depth by a diver welder

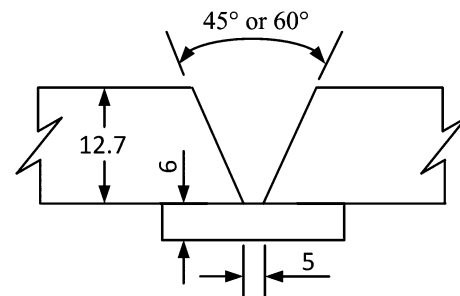


Fig. 1 Groove detail (all dimensions in millimeters)

backing bar (280 mm × 80 mm × 10 mm). V-grooves with 40° or 60° were prepared, and the root opening was 5 mm. The groove detail is shown in Fig. 1. Prior to welding, the surface of the base metal was cleaned to remove any impurities such as oil, rust, or dirt. DCEP current polarity was used. All beads began at the same side of the groove.

Automatic welding experiments were performed by an underwater wet welding system that was developed at Tianjin University in 2013. The system could keep arc length almost constant by an arc voltage feedback controlling system. A hyperbaric chamber with compressed air was used to simulate the different water depths. The inside diameter of the chamber was 2 m, and the length was 3 m. The maximum work pressure was up to 3.0 atm. Lights and cameras, which could withstand work pressure, were placed in the chamber, and testers could observe and record the inside welding process.

Table 1 Chemical composition (wt%)

Material	C	Si	Mn	Al	Nb	V	Cr	Ni	Cu	Ti	CE*
DH36	0.13	0.18	1.4	0.02	0.02	0.05	–	–	–	0.012	0.373
X65	0.06	0.2	1.41	0.034	0.04	0.03	0.045	0.02	0.01	0.017	0.313

$$CE = C + M_n/6 + (C_r + M_o + V)/5 + (N_i + C_u)/15$$

* indicates that carbon equivalent (CE) is calculated by IIW equation that's below the table

Table 3 Summary of welding conditions according to water depths

Sample No.	Welding parameters						
	Water depth (m)	Base metal	Welding method	Welding position	Welding current (A)	Welding voltage (V)	Welding speed (mm/min)
A	0.5	DH36	Automatic	1G	150	24–28	150–180
B	0.5	X65	Automatic	1G	150	24–28	150–180
C	2	DH36	Manual	1G	150	24–28	240–280
D	2	DH36	Manual	2G	150	24–28	240–280
E	2	DH36	Manual	3G	150	24–28	240–280
F	2	X65	Manual	1G	150	24–28	240–280
G	2	X65	Manual	2G	150	24–28	240–280
H	2	X65	Manual	3G	150	24–28	240–280
I	11	DH36	Manual	3G	150	24–28	240–280
J	25	DH36	Automatic	1G	150	24–28	150–180
K	45	DH36	Automatic	1G	150	24–28	150–180
L	55	DH36	Automatic	1G	150	24–28	150–180

2.2 Experimental Scheme

Table 3 shows the experiment scheme in this study. For convenience, in this discussion, the specimens were named A ~ K according to the different conditions. Welding experiments at 2 m were performed by weld-diver in a tank with the size of 2.5 m (length) × 2.5 m (width) × 3 m (height). The welding experiment at 11 m depth was conducted by diver welder in Bohai Sea. The welding experiments at water depths greater than 11 m were carried out in a hyperbaric chamber filled with compressed air.

The cross-sectional observations were firstly performed to inspect the weld defects. Quantitative porosity analysis was performed by optical metallographic measurements in the transverse section. Subsequently, microstructure and weld defects examinations were performed using an OLYMPUS GX51 optical microscope. The chemical composition was measured using an Agilent 725-ES inductively coupled plasma optical emission spectrometry (ICP-OES).

All specimens for the mechanical tests were machined according to AWS D3.6 M: 2010 code for class B wet welds. The HV10 hardness tests were performed by a 432SVD Vickers hardness tester. Figure 2 shows the types and dimensions of the specimens for mechanical properties tests. The reduced-section tension specimens (Fig. 2b) were tested using the CSS-44100 universal testing machine with the speed of 7 mm/min. Three-point bend tests (Fig. 2c) were also performed by the CSS-44100 testing machine, and the bend radius is 60 mm. Besides, for each weld, six standard Charpy v-notch samples (Fig. 2a) were

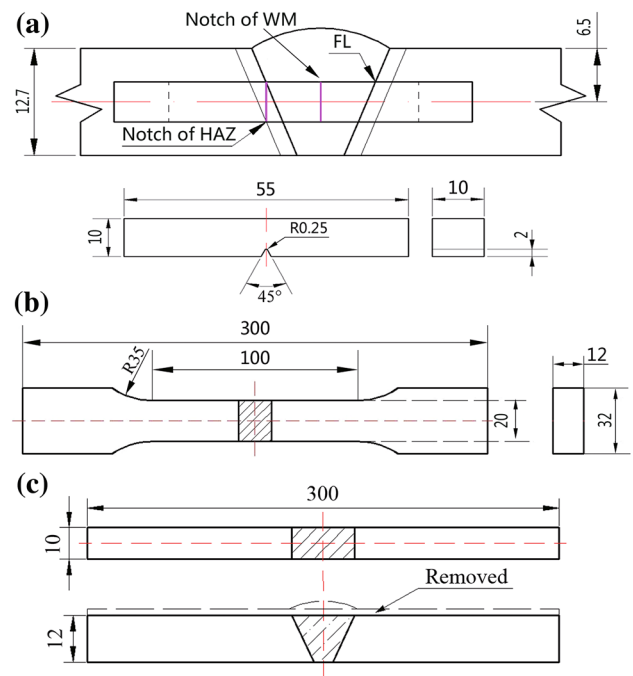


Fig. 2 a Schematic of the Charpy impact specimens: extracted positions and notch locations; schematic of the tensile b and side bend c specimens (all dimensions in millimeters)

extracted and machined to evaluate the impact toughness of the weld metal (WM) and the heat-affected zone (HAZ). Finally, the observations of the fracture surfaces were performed using a Hitachi-S4800 field emission scanning electron microscope.

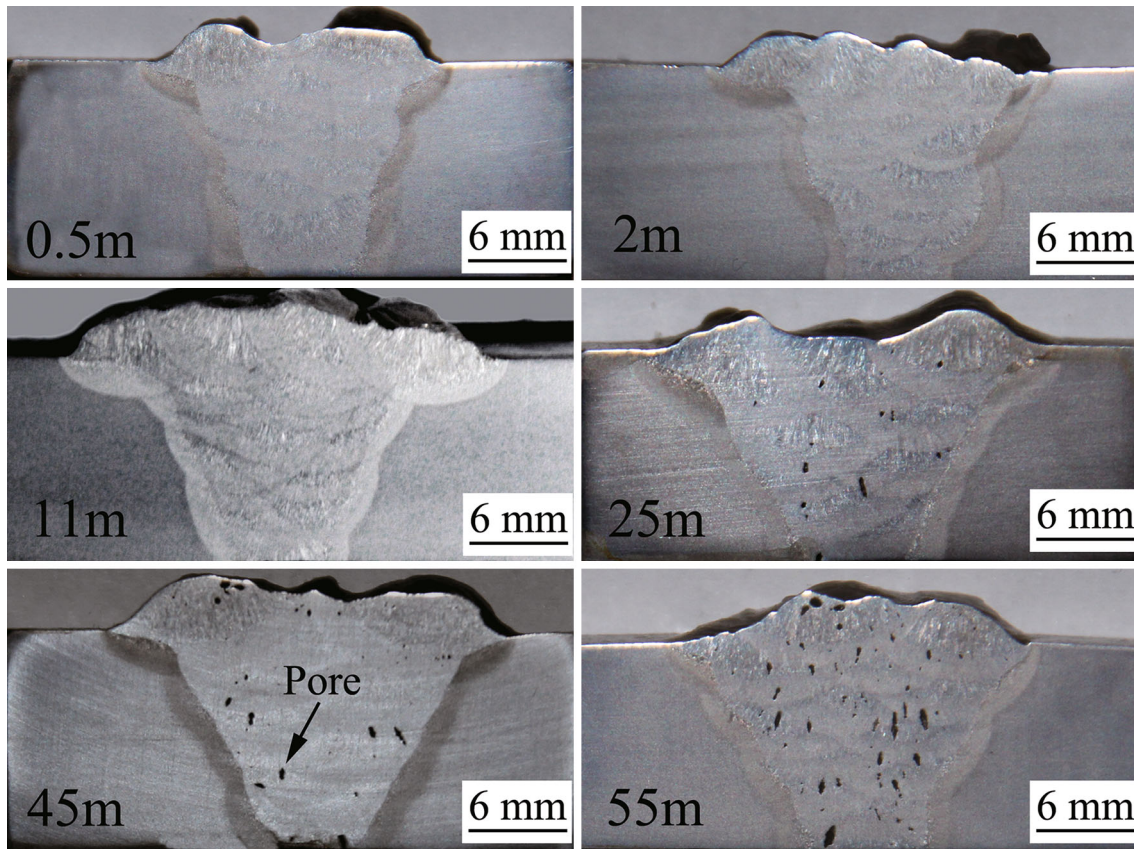


Fig. 3 Cross-sectioning observations of the joints

3 Results and Discussion

3.1 Cross-Sectioning Observations

Figure 3 shows the cross-sectional observations of the DH36 V-notch specimens extracted from A, C, I, J, K, and L welds. Defect-free welds could be obtained within 11 m depth. However, when water depth exceeds 11 m, the welding quality is reduced significantly by the porosity defect. Figure 4 shows the statistical results of the cross-sectional porosity levels. It can be found that the porosity increases to 1% at 25 m, 1.5% at 45 m, and 3.5% at 55 m, respectively. Suga and Hasui [11] found that porosity began to appear at depths greater than 4.6 m and exceeded 5% at about 46 m using rutile electrodes. Obviously, the welds investigated in this paper have less porosity. They also found that the composition of gas contained in wet weld porosity is 96% hydrogen with a small amount of carbon monoxide. When the droplets shedding from the electrode tip transfer into the weld pool, hydrogen enriching in the liquid droplet gets into the molten pool and unable to escape due to the fast cooling effect of water, causing the porosity.

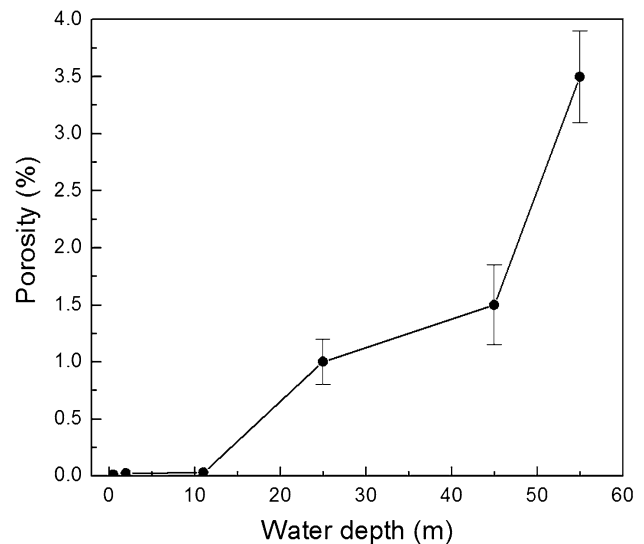


Fig. 4 Statistical results of the cross-sectional porosity of the welds at different depths

Reducing the partial pressure of hydrogen in arc atmosphere can decrease porosity, and this has been verified by Sanchez-Osio *et al.* [12]. They increased calcium carbonate

content of a rutile-base electrode coating from 9 to 12.5% to decrease the porosity from 2.2 to 1.0% at 9 m depth. Carbonates decompose to form carbon dioxide and carbon monoxide, reducing the partial pressure of hydrogen and porosity. In addition, low porosity is associated with the electrodes that deposited a slag with a basicity index approaching neutral, since slag basicity may influence transfer of hydrogen to the weld pool and, thus, influence porosity [13].

3.2 Chemical Composition

Figure 5 reveals the effect of water depth on the main element contents in WM. The carbon content varies slightly ranging from 0.07 to 0.09%, while the oxygen content increases significantly from 0.04% at 0.5 m to 0.09% at 55 m (Fig. 5a). As shown in Fig. 5b, the manganese and silicon contents are 0.47 and 0.32% at 0.5 m and decrease to 0.12 and 0.05% at 55 m depth. It should be noted that the significant drop of manganese and silicon contents happens from 11 to 25 m. The oxidation effect of alloying elements is strengthened by the high concentration of oxygen with increasing depth, leading to manganese and silicon being increasingly partitioned from the weld metal to the slag and oxide inclusions. The variation of alloying elements has a great influence on the microstructures and mechanical properties in WM, and this will be discussed in the later sections.

Figure 6 shows the product of carbon content [C] and oxygen content [O] as a function of water depth. It can be found that there is a linear relationship within 55 m, which is in accordance with the report by Ibarra *et al.* [15]. Carbon monoxide is the product of the decomposition of calcium carbonate in the electrode covering. The carbon

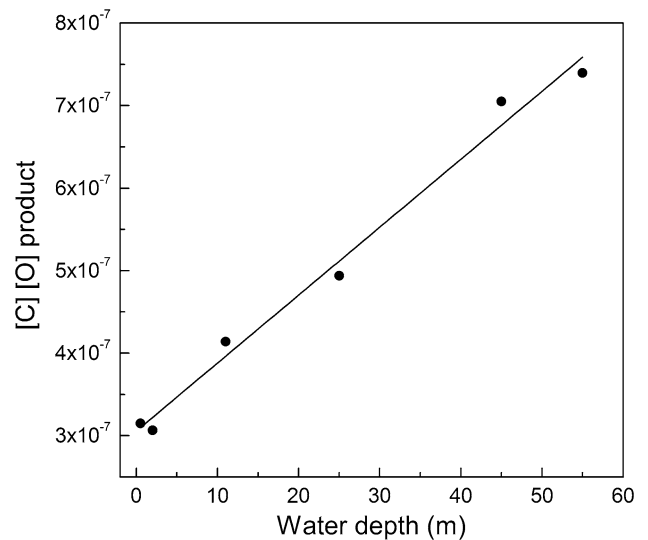


Fig. 6 Product of weld metal carbon and oxygen contents as a function of water depth

monoxide reaction in the arc can be illustrated using the following equations [16].



$$K = \frac{[\text{C}][\text{O}]}{p_{\text{CO}}} \tag{2}$$

$$[\text{C}][\text{O}] = K \cdot p_{\text{CO}} = K \cdot X \cdot p_{\text{total}} = K \cdot X \cdot D = k \cdot D \tag{3}$$

where [C] and [O] are carbon and oxygen contents, respectively, K is the equilibrium constant, p_{CO} is the partial pressure of CO, p_{total} is the total plasma pressure, X is the fraction of weld arc atmosphere, D is the water depth, and k is a constant.

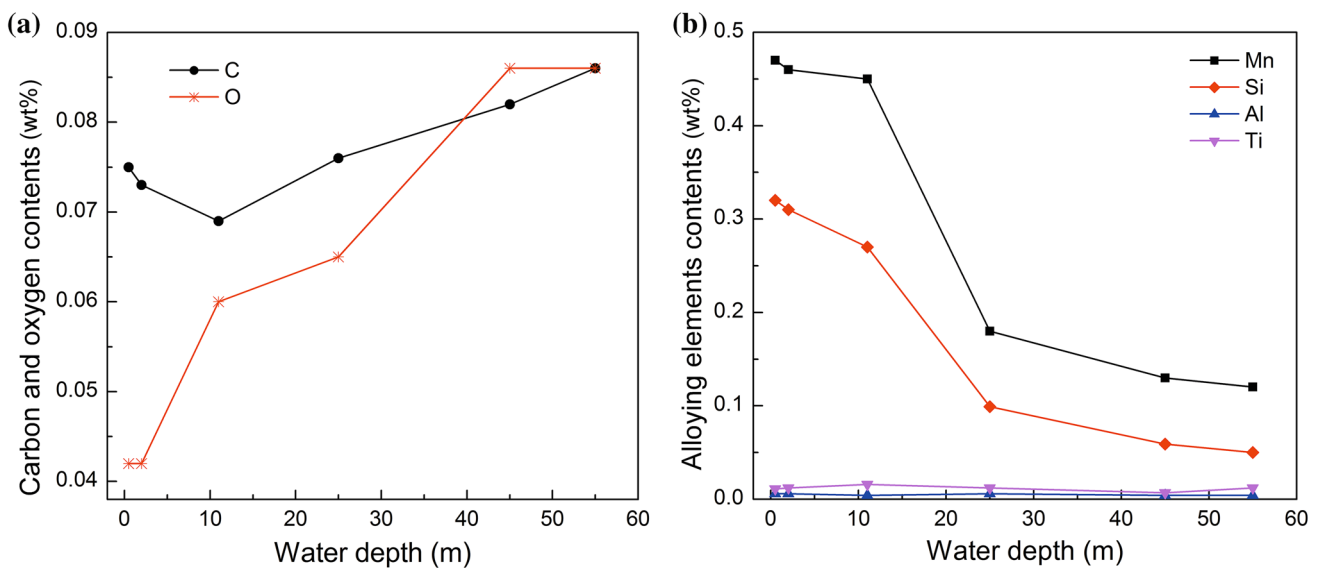


Fig. 5 Effect of water depth on the main element contents in WM: a carbon and oxygen, b alloying elements

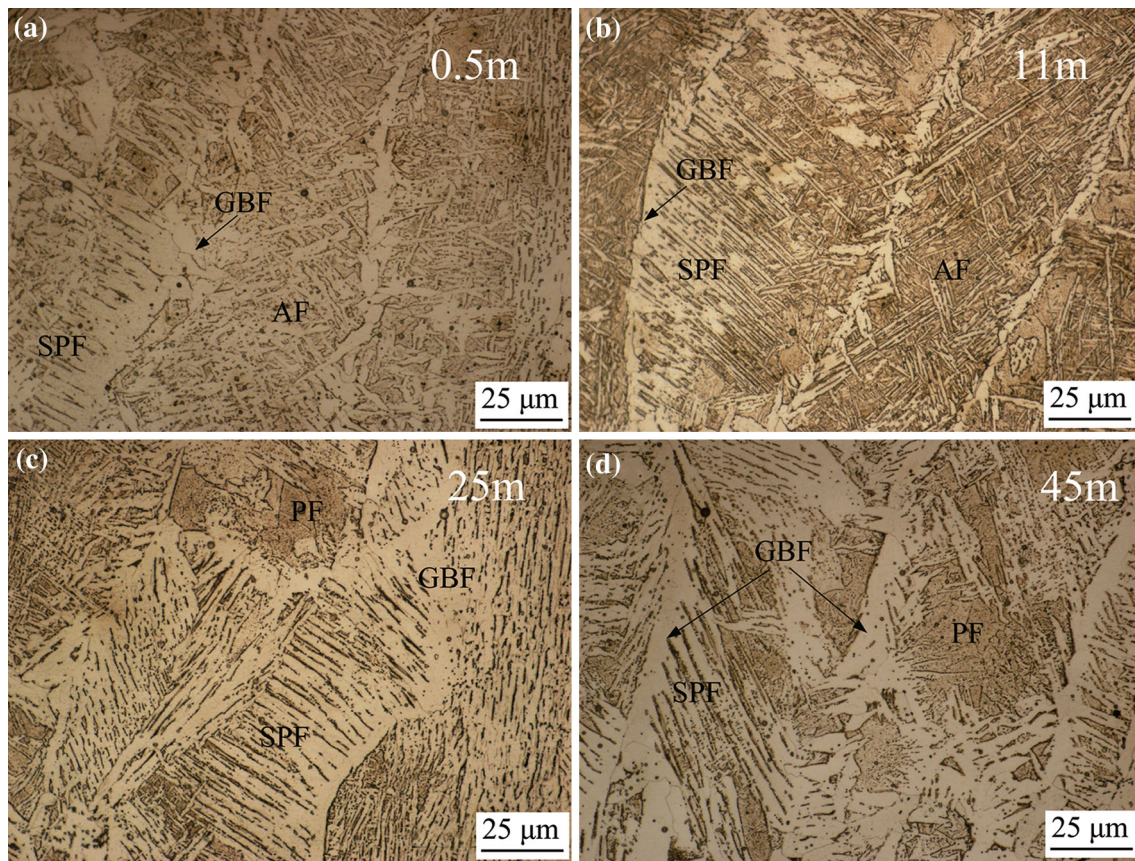


Fig. 7 Typical optical images of columnar microstructures in WM of A, I, J, K welds

The excellent linear relationship shown in Fig. 6 is consistent with Eq. (3), and this demonstrates that the carbon monoxide reaction is controlling the oxygen content within 55 m. Then, the oxygen content will further control the contents of alloying elements by the oxidation reaction.

3.3 Microstructures and Cracks

Figure 7 shows the optical images of columnar microstructure in WM of A, I, J, and K joints. The microstructures mainly consist of the four types of ferrite: grain boundary ferrite (GBF), side-plate ferrite (SPF), acicular ferrite (AF), and polygonal ferrite (PF). The proportion of each type of the ferrite varies with depth. It is recognized that AF is desirable as it provides the maximum resistance to crack propagation [17]. As shown in Fig. 7a, b, the microstructures of A and I welds are characterized by GBF, SPF and AF. A weld has a larger grain size than I weld, and this may contribute to the larger heat input of the former (seen in Table 3). The microstructures of J and K welds are much coarser than those of A and I welds and are mainly composed by GBF, SPF, and PF (Fig. 7c, d).

The loss of alloying elements alters the microstructure in weld metal. Manganese and silicon dissolving in austenite

can enhance the stability of supercooled austenite and delay its decomposition, therefore making the C-curves shift rightward. As discussed before, the alloying element contents decrease with increasing water depth, resulting in C-curves shifting leftward. As a result, for welds at large water depth, the proportion of GBF and PF in the weld increases, while that of SPF and AF decreases.

Figure 8 shows the optical images detailing the HAZ microstructure of DH36 and X65 joint obtained at 0.5 m. The HAZ contains three different regions (Fig. 8a): coarse-grained supercritical HAZ (CGHAZ) encountering temperatures above the recrystallization temperature (typically 1000 °C) and below the solidus temperature, fine-grained supercritical HAZ (FGHAZ) subjected to peak temperatures below the recrystallization temperature but above the A_{c3} temperature, and inter-critical HAZ (ICHAZ) that experienced temperature between A_{c1} and A_{c3} . The CGHAZ of DH36 (Fig. 8b) joint is characterized by almost totally lath martensite, and X65 joint (Fig. 8c) includes lath martensite and upper bainite (UB) with parallel laths. In the heating process of base metal, it is the pearlite that first transforms into austenite and then the ferrite begins to transform. Due to the short heating time of the thermal cycle, the ferrite in BM cannot transform into austenite

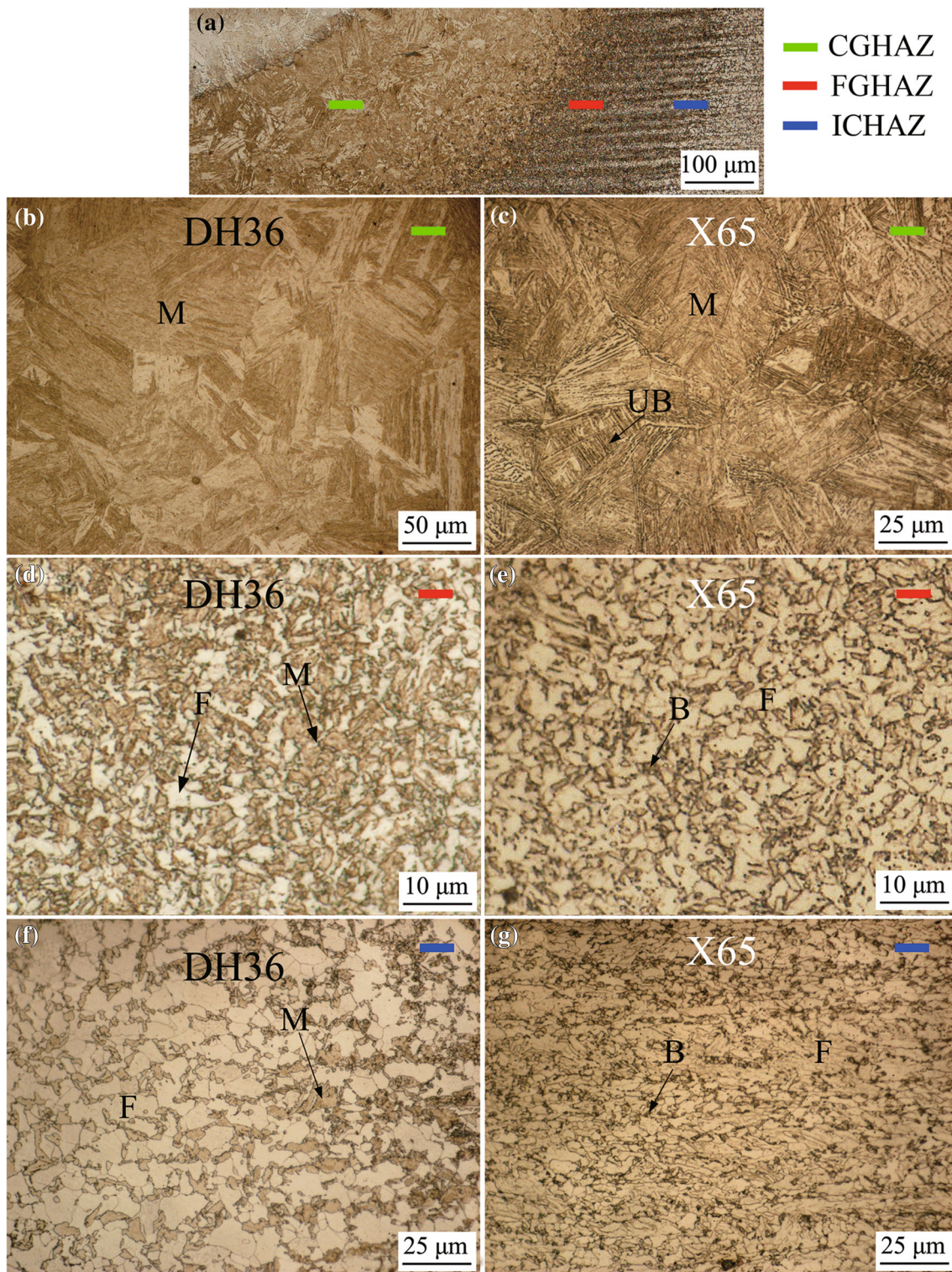


Fig. 8 a HAZ containing three different regions, and HAZ microstructures of the DH36 **b, d, f** and X65 **c, e, g** weld joints. Green, red, and blue marked squares denote the region of CGHAZ, FGHAZ, and ICHAZ, respectively

totally and the untransformed ferrite can be seen in the FGHAZ and ICHAZ. The FGHAZ (Fig. 8d) and ICHAZ (Fig. 8f) of DH36 joint are composed by preexisting ferrite

and martensite, while those of X65 joint (Fig. 8e, g) mainly include ferrite and bainite at the ferrite grain boundary. The sizes of the grains in ICHAZ vary greatly since only partial

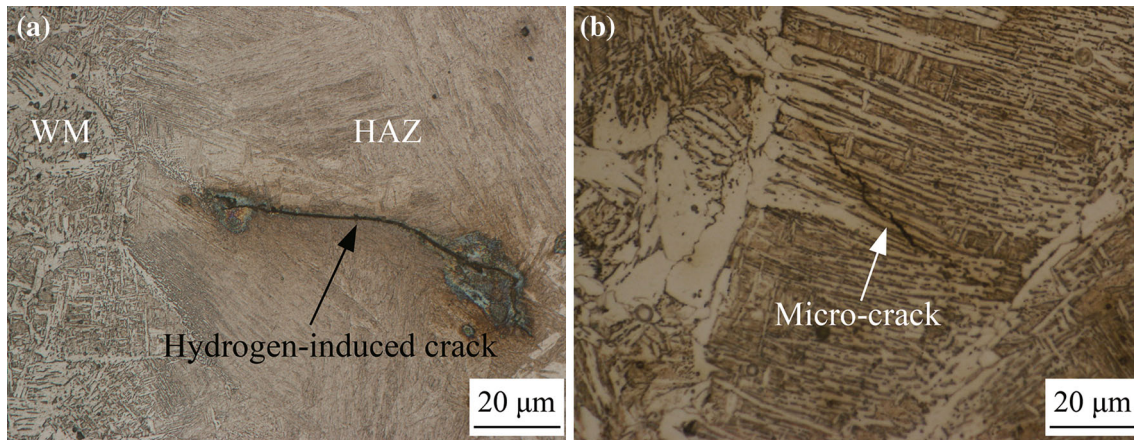


Fig. 9 Typical crack morphology in CGHAZ **a**, WM **b**

ferrite transforms into austenite and then decomposes to fine martensite and bainite, while the ferrite unable to transform into austenite becomes the coarse grains due to grain growth in the heating process. It should be noted that since X65 has lower carbon content and more alloying elements such as Ti, V, and Nb, which act as solution atoms or precipitation to effectively suppress the recrystallization and grain growth of austenite, the grain size in HAZ of X65 joint is much smaller than that of DH36 joint.

Figure 9 depicts the typical cracks in underwater wet joint. Figure 9a shows a hydrogen-induced crack in CGHAZ of DH36 joint because of the hard martensite microstructure, high diffusible hydrogen, and tensile residual stress. Figure 9b reveals a typical microcrack in WM, which usually locates at the brittle SPF microstructure.

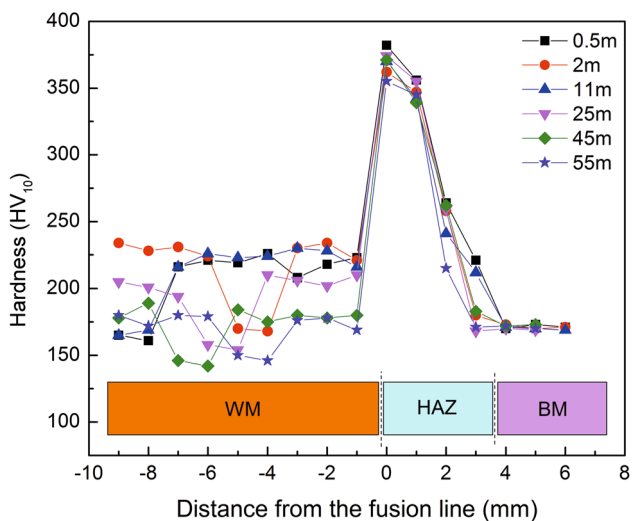


Fig. 10 Hardness distribution of the joints welded at different water depths

3.4 Mechanical Properties

3.4.1 Hardness

Figure 10 shows the hardness variation along the line at the distance of 1 mm from the upper surfaces of the samples extracted from A, C, I, J, K, and L welds. The highest hardness values of 355–382 HV₁₀ are found at CGHAZ close to the fusion line, where large amounts of lath martensite predominate as shown in Fig. 8a. It seems that the water depth has no influence on the highest hardness value. The highest hardness value is limited to 375 HV₁₀ for class B weld according to AWS standard. Thus, hydrogen-induced crack is easy to exist in CGHAZ owing to the high hardness (seen in Fig. 9a). In WM, the hardness distribution varies with the microstructures that exhibit heterogeneous features due to the thermal treatment of the following weld passes. In the columnar grain zone of WM,

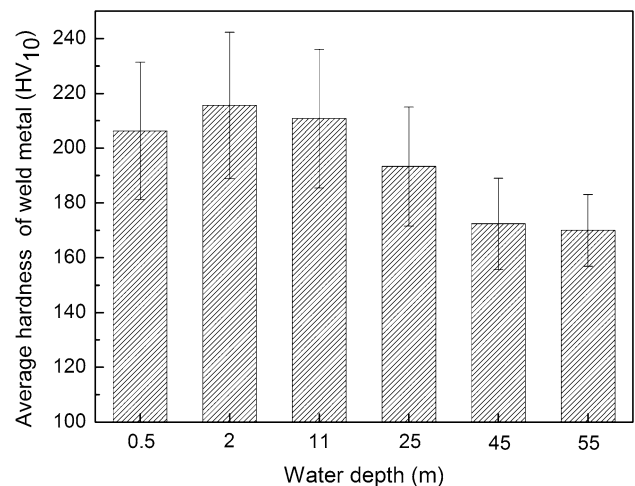


Fig. 11 Average hardness values in WM of the DH36 joints welded at different water depths

most of the hardness values are in the range of 170–230 HV₁₀. However, in the reheating zone of WM where fine polygonal ferrite predominates, the hardness values range from 140 to 170 HV₁₀.

To investigate the influence of water depth on the hardness in WM, the average hardness values are calculated and shown in Fig. 11. It can be seen that the C weld obtained at 2 m has the highest average hardness value. This may contribute to the sufficient manganese and silicon elements (Fig. 5b) and the lower heat input as illustrated in Table 3. Both of the two factors can strengthen the weld metal. Then, the average hardness value decreases with increasing water depth, since large fractions of polygon ferrite can be produced at greater depths due to the loss of alloying elements in WM. When the water depth increases to 45 or 55 m, the average hardness value is about 170 HV₁₀, which is comparable to that of base metal.

3.4.2 Tensile Property, Ductility, and Toughness

The detailed results of the tensile and side bend tests are shown in Table 4. For X65 joints of 0.5 and 2 m, the ultimate tensile strengths (UTS) are in the range of 540–560 MPa and are below that of X65, leading to the fracture at WM. The tensile elongation is about 8%, and almost all of the plastic deformation occurs at WM due to the higher yield strength of X65 steel. For DH36 joints, all of the tensile samples from welds within 11 m depth fracture at BM and the tensile elongations are about 30%. However, all of the specimens extracted from welds at water depth greater than 11 m, fracture at WM, and both of the UTS and elongation decrease with the increasing depth.

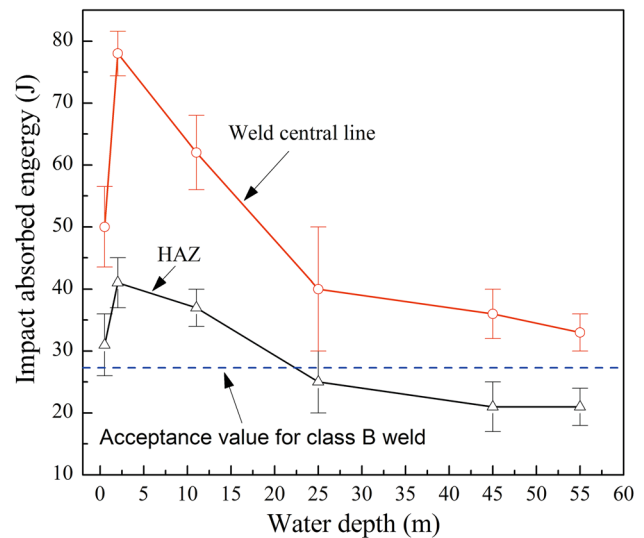


Fig. 12 Charpy impact-absorbed energy of the DH36 joints welded at different water depths

Side bend tests (Table 4) show that the ductility of the joints welded within 11 m depth meets the requirement of class B weld standard except the X65 joints welded at 2G and 3G (down) positions. The failure may result from the high strength of X65 steel and the slag and undercut weld defects, which are largely influenced by welder's skills in these welding positions. When water depth exceeds 11 m, the ductility dramatically gets worse, which is mainly caused by the large amounts of porosity.

Figure 12 shows the impact-absorbed energy of DH36 V-notch impact specimens extracted from A, C, I, J, K, and L welds. The impact energy at WM and HAZ

Table 4 Summary of mechanical properties test results, in which σ_b and δ refer to the ultimate tensile strength and the elongation

Sample No.	Tensile properties		Fracture location		Side bend 6T ^a	Charpy V (J) ^b	
	σ_b (MPa)	δ (%)	BM	WM		WM	HAZ
A	538	30	✓		4/4	31	50
B	552	7.2		✓	4/4	32	52
C	542	30	✓		4/4	41	78
D	540	30	✓		4/4	41	72
E	536	30	✓		4/4	41	75
F	555	7.8		✓	4/4	43	74
G	550	7.9		✓	0/4	42	67
H	558	8.5		✓	0/4	41	78
I	540	30	✓		4/4	37	62
J	511	15		✓	2/4	25	40
K	493	14		✓	1/4	21	36
L	478	12		✓	0/4	21	33

BM, WM, and HAZ mean the base metal, weld metal, and heat-affected zone, respectively

^a Number of approvals/number of tests. ^b Tested at 0 °C

exhibits similar variation tendency. The best one is found at 2-m weld, which has the highest impact energy of 41 J at WM and 68 J at HAZ. Then, the absorbed energy decreases with increasing depth. L weld at 55 m exhibits the lowest impact energy of 21 J at WM and 33 J at HAZ. Besides, impact toughness of the welds within 11 m meets the

requirement of class B weld (a minimum value of 27 J, according to AWS [10]). What is more, 0.5-m weld seems to have inferior toughness than 2-m weld, which can be explained by the arc stability and the welding heat input. Firstly, 0.5-m welds would result in unstable arc and more weld defects compared with 2-m welds. On the other hand,

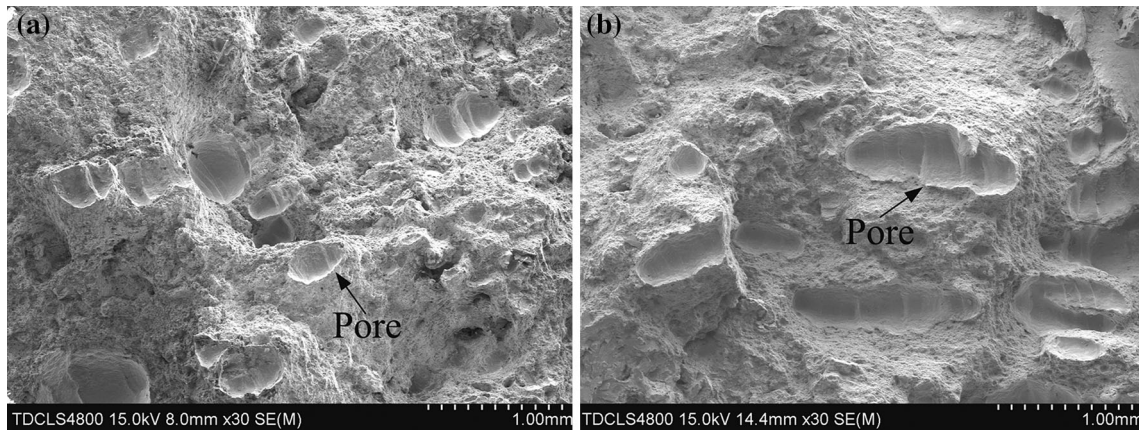


Fig. 13 Typical pore morphology in DH36 Charpy impact samples after fracture: **a** 25 m, **b** 45 m

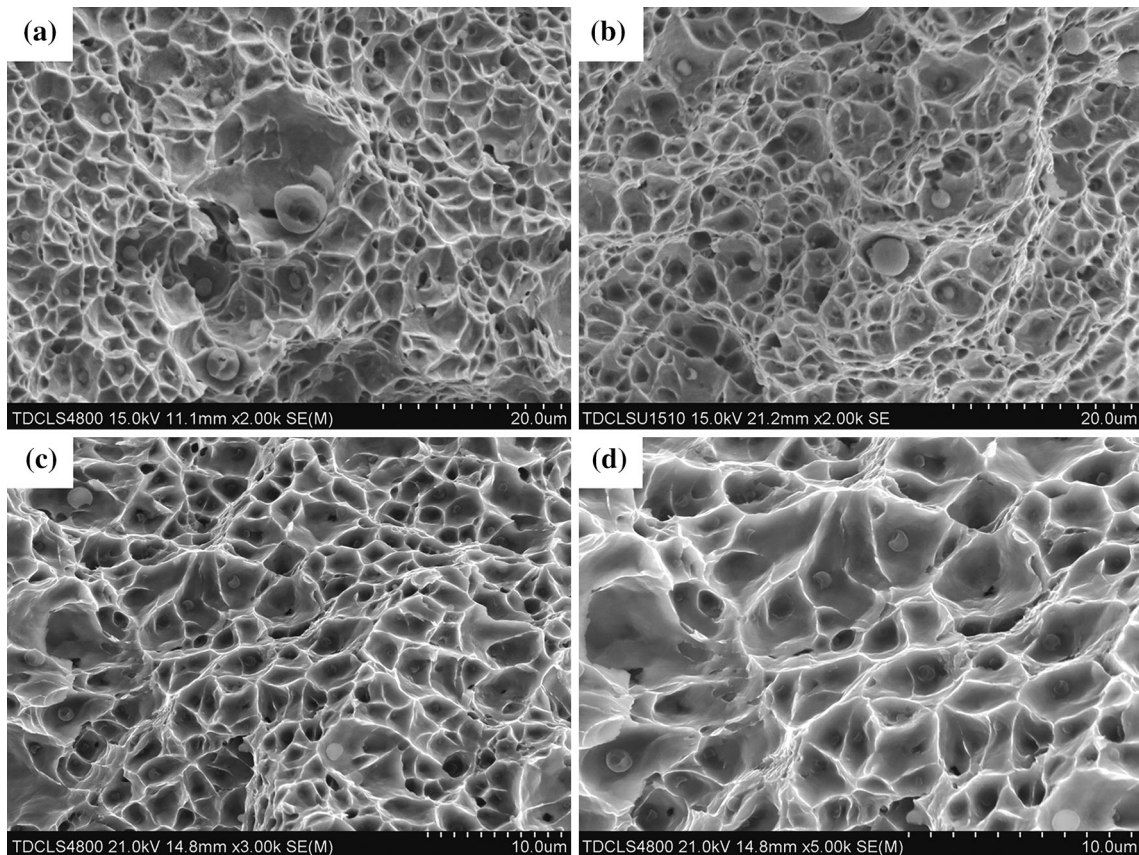


Fig. 14 Fracture morphology of the weld metal for the impact specimens that were welded at 2 m **a**, 11 m **b**, 25 m **c**, 45 m **d** depth

2-m welds have more volume fractions of the fine grain region than 0.5-m welds since the former is filled by 24 passes due to the smaller heat input, while the latter is filled by 12 passes.

3.4.3 Fracture Morphology

Figure 13 shows the typical pore morphologies in 25- and 45-m impact samples after fracture. Obviously, 45-m weld (the pore length is about 0.5 mm) has a larger pore than 25-m weld (the length is about 1.2 mm), owing to the larger hydrostatic pressure prohibiting the escape of hydrogen in molten pool. The pores in 25-m welds are close to axiolytic shape and caterpillar-shape in 45-m welds.

Figure 14 shows typical SEM impact fracture morphologies at the weld metal (WM) of the specimens. All of the fracture surfaces are full of dimples with different sizes, indicating a significant characteristic of void nucleation and coalescence. Oxide inclusions act as sites for initiation of the void coalescence. Despite the seeming ductile fracture mechanism, the fine and shallow equal-axis dimples, indicative of a large amount of oxide inclusions and the large hardening exponent, correspond to the low impact energy. Energy-dispersive X-ray spectroscopy (EDS) was used to determine the chemical composition of the non-metallic inclusions, and the representative result is shown in

Table 5 EDS result of a typical nonmetallic inclusion in 25-m DH36 weld

EDS result	C	O	Al	Si	Ti	Mn	Fe
Weight (%)	4.58	39.86	1.1	27.59	6.06	15.91	4.9
Atom number (%)	8.68	56.63	0.92	22.33	2.87	6.58	2

Table 5. The inclusion was found to be enriched with O, Si, Mn, and Ti. It is supposed that the main types of inclusions are SiO₂ and MnO. Besides, the test results correspond to the lower oxidizing potential of rutile electrodes used in this research compared with oxide electrodes [14].

3.4.4 Discussion About Mechanical Properties

In all, mechanical properties of underwater wet welds are a strong function of depth. Welds within 11 m have good mechanical properties and can meet the requirements about class B weld of AWS D 3.6 standard. However, when depth exceeds 11 m, changes in microstructure, chemical composition, microcracks, and porosity undoubtedly contribute to the decline in the mechanical properties. The decrease in alloying element contents reduces the hardenability of the weld metal and promotes coarse-grained primary ferrite. Also, porosity reduces the effective bearing area, causing lower strength and toughness.

Table 6 presents a review about the composition and the mechanical properties as a function of water depth. It can be seen that the experimental results in this study are consistent with other researchers' using rutile electrodes with similar chemical compositions [13, 18]. In order to overcome the problem of alloying elements loss, Rowe *et al.* [13] added a strong deoxidant (titanium and boron) to protect manganese from oxidation. Additions of titanium and boron are effective for refining the ferrite grain size and can act as nucleation sites to promote the production of acicular ferrite [17]. However, the additions did not significantly improve the impact toughness (Table 6). The toughness of wet welds is most likely controlled by the concentration of the defects, such as pores, microcracks, and oxide inclusions [13].

Table 6 Chemical composition and mechanical properties of underwater wet welds as a function of depth (reported in the literature)

Reference	Depth (m)	Chemical composition (wt%)				Transversal tension UTS (MPa)	All-weld-metal tension		Impact energy (J, 0 °C)
		C	Mn	Other elements			UTS (MPa)	Elongation (%)	
Pope <i>et al.</i> [19]	1	0.05	0.03	Ni	2	465	–	–	50
Santos <i>et al.</i> [14]	10	0.05	0.05	Ni/Mo	2.37/0.18	527	547	14.4	42
Pope <i>et al.</i> [19]	12	0.03	0.02	Ni	2	434	–	–	35
Pope <i>et al.</i> [19]	20	0.04	0.02	Ni	2	445	–	–	33
Rowe <i>et al.</i> [13]	21	0.04	0.69	Si	0.3	0	489	18.6	39
Rowe <i>et al.</i> [13]	21	0.05	1.03	Ti/B	0.033/0.0022	0	489	4.2	30
Rowe <i>et al.</i> [13]	43	0.05	0.49	Si	0.21	0	448	11.7	34
Rowe <i>et al.</i> [13]	43	0.05	0.51	Ti/B	0.0095/0.0014	0	551	3.7	35
Szelagowski <i>et al.</i> [18]	55	0.16	0.46	Si	0.42	438	–	–	28
Szelagowski <i>et al.</i> [18]	55	0.15	0.2	Si	0.14	383	363	–	24
Rowe <i>et al.</i> [13]	61	0.05	0.47	Si	0.26	0	407	3.6	31
Rowe <i>et al.</i> [13]	61	0.05	0.6	Ti/B	0.0075/0.0008	0	469	6.4	30

Ferritic electrodes are commonly used in underwater wet welding and are divided into two groups: rutile electrodes and oxidizing electrodes. The former has good arc stability and low ductility, while the latter has low diffusible hydrogen content (low cracking susceptibility and high ductility) but poor operability [14]. Santos *et al.* [14] developed an oxyrutile electrode for wet welding up to 20 m depth, combining the advantages of the two types of electrodes. Nickel and molybdenum were added to strengthen the weld metal. The oxyrutile electrodes show lower porosity and have superior toughness and ductility. In particular, the excellent ductility within 20 m can meet the requirement of class A weld.

4 Conclusions

1. With increasing water depth, the contents of alloying elements decrease and the oxygen content increases. The significant drop of manganese and silicon contents happens from 11 to 25 m. Within 55 m water depth, the carbon monoxide reaction controls the oxygen content, which will further control the contents of alloying elements by oxidation reaction.
2. The columnar microstructures in WM of welds obtained at shallow water consist of the grain boundary ferrite, side-plate ferrite, and the acicular ferrite, while those of welds welded at the depth greater than 25 m exhibit more proeutectoid ferrite and less acicular ferrite since the C-curves shift leftward due to the loss of alloying elements.
3. Mechanical properties of underwater wet welds are a strong function of depth owing to the increase in the oxidation of alloying elements and porosity. Welds obtained within 11 m depth show preferable strength, ductility, and toughness. The mechanical properties sharply drop from 11 to 25 m because of the increasing porosity and oxidation of alloying elements.

Acknowledgments The authors acknowledge the financial support of marine scientific research project (investigate on the key

technology of underwater welding and inspection processes-developing special machines and processes for local dry and wet underwater welding) sponsored by Offshore Oil Engineering Co., Ltd. Great thanks are given to Jun Cao and Wei Xu from Offshore Oil Engineering Co., Ltd.

References

- [1] F.L. Sun, X.L. Li, F. Zhang, X.Q. Cheng, C. Zhou, N.C. Wu, Y.Q. Yin, J.B. Zhao, *Acta Metall. Sin. (Engl. Lett.)* **26**, 257 (2013)
- [2] S. Atashin, M. Pakshir, A. Yazdani, *Acta Metall. Sin. (Engl. Lett.)* **23**, 161 (2010)
- [3] B. Zhao, C.S. Wu, C.B. Jia, X. Yuan, *Acta Metall. Sin.* **49**, 797 (2013). (in Chinese)
- [4] J.E. Rodriguez-Sanchez, F. Perez-Guerrero, S. Liu, A. Rodriguez-Castellanos, A. Albitier-Hernandez, *Fatigue Fract. Eng. Mater. Struct.* **37**, 637 (2014)
- [5] J.E. Rodriguez-Sanchez, A. Rodriguez-Castellanos, F. Perez-Guerrero, M.F. Carbajal-Romero, S. Liu, *Fatigue Fract. Eng. Mater. Struct.* **34**, 487 (2011)
- [6] M. Rowe, S. Liu, *Sci. Technol. Weld. Join.* **6**, 6 (2001)
- [7] E.C.P. Pessoa, A.Q. Bracarense, E.M. Zica, S. Liu, F. Perez-Guerrero, *J. Mater. Process. Technol.* **179**, 239 (2006)
- [8] F. Perez, S. Liu, C. Smith, E. Rodriguez, in *22nd International Conference on Offshore Mechanics and Arctic Engineering* (Mexico, 2003)
- [9] H.T. Zhang, X.Y. Dai, J.C. Feng, L.L. Hu, *Weld. J.* **94**, 8s (2015)
- [10] American Welding Society, Underw. Weld Code AWS D **3(6M)**, 2010 (2010)
- [11] Y. Suga, A. Hasui, *Trans. Jpn. Weld. Soc.* **17**, 58 (1986)
- [12] A. Sanchez-Osio, S. Liu, S. Ibarra, *J. Offshore Mech. Arct.* **117**, 212 (1995)
- [13] M.D. Rowe, S. Liu, T.J. Reynolds, *Weld. Res.* **156-s** (2002)
- [14] V.R. Santos, M.J. Monteiro, F.C. Rizzo, A.Q. Bracarense, E.C.P. Pessor, R.R. Marinho, L.A. Vieira, *Weld. J.* **91**, 319 (2012)
- [15] S. Ibarra, C.E. Grubbs, D.L. Olson, *J. Met.* **12**, 8 (1988)
- [16] O. Grong, D.L. Olson, N. Christensen, *Met. Construct.* **12**, 810 (1985)
- [17] S.S. Babu, *Curr. Opin. Solid State Mater.* **8**, 267 (2004)
- [18] P. Szlagowski, I. Pachniuk, H. Stuhff, *Proceedings of the Second International Offshore and Polar Engineering Conference* (San Francisco, 1992)
- [19] A.M. Pope, C.G. Teixeira, M.P. Paes, V.R. Santos, D. Ros, J.R. Domingues, *Proceedings of 16th Offshore Mechanics and Arctic Engineering Conference* (American Society of Mechanical Engineers, 1997)